Irish Interdisciplinary Journal of Science & Research (IIJSR)
Volume 7, Issue 2, Pages 84-95, April-June 2023

Application of Time-Frequency Decomposition and Seismic Attributes for Stratigraphic Interpretation of Thin Reservoirs in Onshore Fuba Field Niger-Delta, Nigeria

U. Ochoma*

Department of Physics, Rivers State University, P.M.B 5080, Port Harcourt, Nigeria.
*Email: umaocho@gmail.com**

DOI: https://doi.org/10.46759/IIJSR.2023.7210

Article Received: 13 April 2023 *Article Accepted: 22 May 2023* *Article Published: 10 June 2023*

ABSTRACT

Application of time-frequency decomposition and seismic attributes for stratigraphic interpretation of thin reservoirs in Onshore Fuba Field Niger Delta, Nigeria, are here presented, using Well-log and 3D Seismic data. Well-to-seismic tie, fault mapping, horizon mapping, time surface generation, depth conversion and seismic attributes generation were carried out using Petrel software. Structural interpretation of seismic data reveals a highly faulted field. Two distinct horizons were mapped. Fault and horizon interpretation shows closures that are collapsed crestal structures bounded by two major faults. All the interpreted faults are normal synthetic and antithetic faults which are common in the Niger Delta basin. The depth structure maps reveal anticlinal faults. Reservoirs are found at a shallower depth from 6500 to 7500 ft and at a deeper depth ranging from 11500 to 13000 ft. The variance and chaos values range from 0.0 to 1.0. The Variance edge and chaos analysis were used to delineate the prominent and subtle faults in the area while the produced spectra were used to delineate the stratigraphy and thickness of the thin-bedded reservoirs. The results of spectral decomposition at frequencies between 12Hz and 35Hz indicate some thin pay sand zones reservoirs which were characterized by of low frequency and high amplitude associated with known hydrocarbon zones, meandering channels, lobes and the presence of small scale faults in the field. Six new probable zones (Prospects A, B, C, D, E and F) of hydrocarbon accumulation were identified. The results of the study will help in the recovery of more hydrocarbon as by-passed zones and subtle structures are revealed in the area of study.

Keywords: Seismic, Fourier transform, Spectral decomposition, Meandering channels, Niger Delta, Nigeria.

1.0. Introduction

Spectral decomposition is the use of small or short windows for transforming and displaying frequency/ wavenumber spectra (Sheriff, 2002). Spectral analysis has been one of the significant interpretation methods in seismic analysis because seismic data is non-stationary in nature (Bayowa, et al, 2021). In conventional seismic interpretation, seismic signals are only expressed in time domain with little or no emphasis on the inherent seismic amplitude variations, which could have been used to analyze the stratigraphy (Helal, et al, 2015; Rotimi et al, 2010).

In the Niger Delta, it may be challenging to plot thin reservoirs using this traditional method, where there are successive intercalations of sand and shale within the petroliferous paralic Agbada formation for thick reservoir mapping (Doust, and Omatsola, 1990). The low frequency with longer wavelength penetrates better for thick reservoirs but the high frequency with short-wavelength probes deeper for a thinly bedded reservoir (Oluwadare, et al, 2020). When the structure is complex, subtle structures may not be detected on the seismic data due to the fact that seismic data is band limited and has a limited vertical resolution. Compared with horizon based slices in time domain, spectral analysis provides better vertical resolution of various depositional features on frequency slices (Naseer, and Asim, 2018; Tayyab, et al, 2017).

Spectral decomposition can be done by using different methods such as short window discreet Fourier transform, Continuous wavelet transform, stock-well transform, matching pursuit or by using Fast Fourier Transform (Castagna, and Sun, 2006). The information could be used to detect, characterize, predict and keep under surveillance the hydrocarbon reservoirs (Taner et al, 1979). Several researchers have made enormous contributions

based on spectral analysis within the Niger Delta basin to investigate the potentiality of hydrocarbon deposits. Marfurt, and Kirlin, (2001) used the Discrete Fourier Transform to map time thicknesses. Sinha et al, (2005) applied spectral decomposition as a direct hydrocarbon indicator. Tomasso, et al, (2010) used spectral re-composition to recover the frequencies and its associated amplitudes (weights) as a reversed problem by an improved formula.

This study is taken from Fuba Field, Depobelt, Niger Delta, Nigeria. The ultimate deliverable of this study was application of time-frequency decomposition and seismic attributes for stratigraphic interpretation of thin reservoirs. The major components of this study are: (a) Well Correlation performed in order to determine the continuity of the reservoir sand across the field. (b) Seismic Interpretation which involves well-to-seismic tie, fault mapping, horizon mapping, time surface generation, depth conversion and seismic attributes generation. This aids in giving more insight into application of time-frequency decomposition and seismic attributes for stratigraphic interpretation of thin reservoirs. in onshore Fuba field Niger-Delta, Nigeria.

2.0. Location and Geology of the Study Area

The proposed study area Fuba Field is located in the onshore Niger Delta region. Figure 1 shows the map of the Niger Delta region showing the study area. The Niger Delta lies between latitudes 4° N and 6° N and longitudes 3° E and 9° E (Whiteman, 1982). The Delta ranks as one of the major oil and gas provinces globally, with an estimated ultimate recovery of 40 billion barrels of oil and 40 trillion cubic feet of gas (Adegoke, et al., 2017). The coastal sedimentary basin of Nigeria has been the scene of three depositional cycles (Short, and Stauble, 1967).

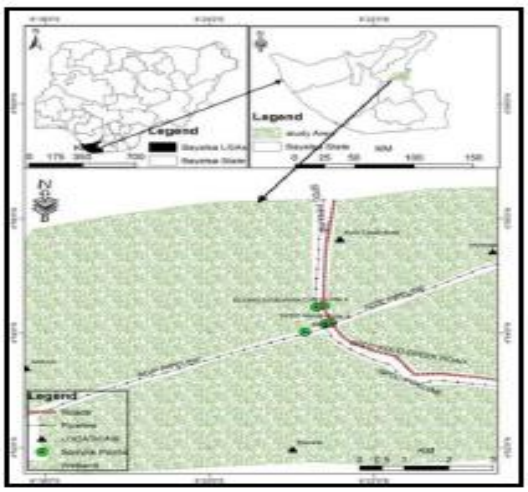

Figure 1. Map of Niger Delta Oilfields showing the location of Fuba Field

The first began with a marine incursion in the middle Cretaceous and was terminated by a mild folding phase in Santonian time. The second included the growth of a proto-Niger delta during the Late Cretaceous and ended in a major Paleocene marine transgression. The third cycle, from Eocene to Recent, marked the continuous growth of the main Niger delta. A new threefold lithostratigraphic subdivision is introduced for the Niger delta subsurface, comprising an upper sandy Benin Formation, an intervening unit of alternating sandstone and shale named the Agbada Formation, and a lower shaly Akata Formation. These three units extend across the whole delta and each ranges in age from early Tertiary to Recent. They are related to the present outcrops and environments of

deposition. A separate member of the Benin Formation is recognized in the Port Harcourt area. It is Miocene-Recent in age with a minimum thickness of more than 6,000ft (1829m) and made up of continental sands and sandstones (>90%) with few shale intercalations (Horsfall, et al., 2017). Subsurface structures are described as resulting from movement under the influence of gravity and their distribution is related to growth stages of the delta (Ochoma, et al., 2020). Rollover anticlines in front of growth faults form the main objectives of oil exploration, the hydrocarbons being found in sandstone reservoirs of the Agbada Formation.

3.0. Methodology

3.1. Well-Log and Seismic Data Quality Control

Well correlation is the first stage of the pre-interpretation process. The process of well correlation involves lithologic description, picking top and base of sand-bodies, fluid discrimination and then linking these properties from one well to another based on similarity in trends. In between these two lithologies in the subsurface, the gamma ray log is often used. Correlation of reservoir sands was achieved using the top and base of reservoir sands picked. The correlation process was possible based on similarity in the behavior of the gamma ray log the Niger Delta; the predominant lithologies are sands and shales. In order to discriminate shapes. Also, the thickness of the shale bodies overlying and underlying the sand body is considered during Correlation. After defining the lithologies, the resistivity log was used for discriminating the type of fluid occurring within the pores in the rocks.

There are seven basic steps involved in seismic interpretation relevant to this study and they include; Well-to-seismic ties, Fault Mapping, Horizon mapping, Time surface generation, Velocity Modelling, Depth Conversion and attributes generation. Well-to-seismic tie is a process that enables the visualization of well information on seismic data. For this process to be achieved, the following are basic requirements; checkshot, sonic log, density log and a wavelet. The sonic log, which is the reciprocal of velocity, was calibrated using the checkshot data. The calibration process is necessary in order to improve the quality of the sonic log because the sonic log is prone to washouts and other wellbore related issues. The results of calibrating the sonic log with the checkshot gives a new log called the calibrated sonic log.

The calibrated sonic log is used along with the density log to generate an acoustic impedance (AI) log. The acoustic impedance log is calculated for each layer of rock. The next step involves generating the reflectivity coefficient (RC) log. The RC is calculated and generated using the AI log. The RC log generated is then convolved with a wavelet to generate a synthetic seismogram which is comparable with the seismic data. The statistical wavelet utilized for convolution is extracted from the seismic data. The synthetic seismogram was generated for every well that had checkshot, density and sonic log. The reflections on the synthetic seismogram were matched with the reflections on seismic data. The mathematical expressions that governs the entire well-to-seismic tie workflow are presented below;

$$AI = \rho v \qquad (1)$$

$$RC = \frac{\rho_2 v_2 - \rho_1 v_1}{\rho_2 v_2 + \rho_1 v_1} \qquad (2)$$

$$\textit{Synthetic Seismogram} = \frac{\rho_2 v_2 - \rho_1 v_1}{\rho_2 v_2 + \rho_1 v_1} * wavelet \qquad (3)$$

Where ρ= Density, v =Velocity, AI= Acoustic impedance and RC = Reflection coefficient.

Faults were identified as discontinuities or breaks in the seismic reflections. Faults were mapped on both inline and cross-line directions. Horizons are continuous lateral reflection events that are truncated by fault lines. The horizon interpretation process was conducted along both inline and crossline direction. At the end of the horizon mapping, a seed grid is generated which serves as an input for time surface generation. Time surfaces were generated using the seed grids gotten from the horizon mapping process. The third order polynomial velocity model was generated and used to depth convert the time surfaces of the reservoirs of interest.

3.2. Variance (Edge Detection) Method

The variance attribute is edge imaging and detection techniques. It is used for imaging discontinuity related to faulting or stratigraphy in seismic data. Variance attribute is proven to help in imaging of channels, fault zones, fractures, unconformities and the major sequence boundaries (Pigott. et al, 2013). In the Petrel software, the variance attribute uses an algorithm that computes the local variance of the seismic data through a multi-trace window with user-defined size. The local variance is computed from horizontal sub-slices for each voxel. A vertical window was used for smoothing the computed variance and the observed amplitude normalized. The variance attribute measures the horizontal continuity of the amplitude that is the amplitude difference of the individual traces from their mean value within a gliding CMP window.

$$\sigma^2 = \frac{1}{n}\sum_{f_i=1}^{n}(x_i + x_m)^2 \qquad (4)$$

Where σ = standard deviation, σ^2 = variance, n = the number of observations, f_i = frequency, x_i = the variable, x_m = mean of x_i

3.3. Chaos

Chaos attribute is defined as a measure of the "lack of organization" in the dip and azimuth estimation method. It can be used to distinguish different sediment facies in lithology variation environments (for example, sand and shale).

3.4. Spectral Decomposition

Spectral decomposition is a frequency attribute. It involves separating and classifying seismic events within each trace based on their frequency content. Each 1D trace was decomposed from the time domain into its corresponding 2D representation in the time-frequency domain using algorithms. Once each trace was transformed into the time-frequency domain, a band-pass filter was applied to view the amplitude of seismic data at different frequencies.

The short-time Fourier transform (STFT) spectrogram which is the squared modulus of the STFT and the spectral energy density is defined as (Cohen, 1989).

$$SP_s(t, f) = /\int_{-\infty}^{\infty} s(\tau)h(\tau - t)e^{-j2\pi f\tau}d\tau\,/^2 \qquad (5)$$

Where, $h(\tau - t)$ = the window function, $s(\tau)$ = the signal, SP_s = the short-time Fourier transform, j = the imaginary unit, τ = the time delay.

The relationships between the amplitude spectrum ($A(w)$) and the phase spectrum ($\gamma(w)$) of the estimated transformed signals are presented in equations 6 and 7:

$$/A(w^T)/ = \sqrt{A_r + A_i} \qquad (6)$$

$$\gamma(w) = \mathrm{Tan}^{-1}[\frac{A_i}{A_r}] \qquad (7)$$

Where, A_r = real part of $A(w^T)$, A_i = imaginary part of $A(w^T)$, w = frequency, T = transform of the signal, $A(w^T)$ = amplitude of transformed trace at frequency w.

4.0. Results and Discussion

4.1. Reservoir Identification, Correlation and Well-to-Seismic Ties

The results for lithology and reservoir identification are presented in Figure 2. A total of nine sand bodies (A, B, C, D, E, F, G, H and I) were identified and correlated across all seven wells in the field. Two reservoir sands were selected for the purpose of this study (Reservoirs A and I). The resistivity logs which reveals the presence of hydrocarbons were used to identify the hydrocarbon bearing sands.

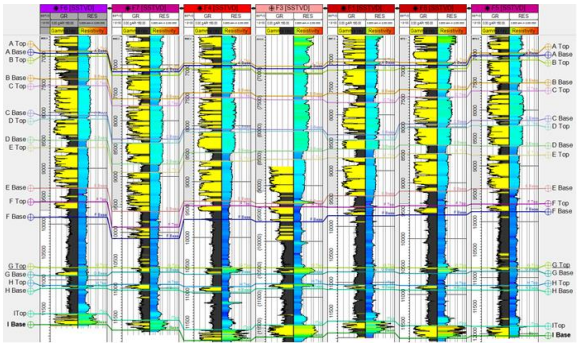

Figure 2. Well section showing reservoir identified and correlated across Fuba Field

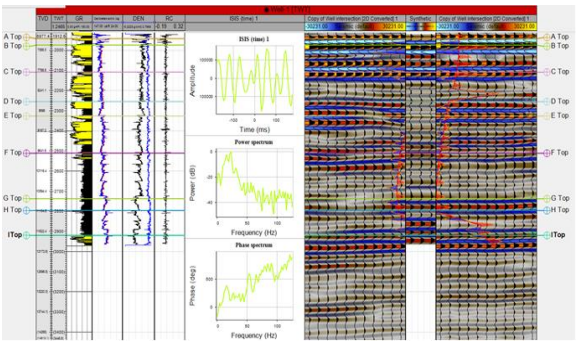

Figure 3. Synthetic seismogram generation and well-to-seismic tie conducted for Fuba Field using Well-1 Checkshot

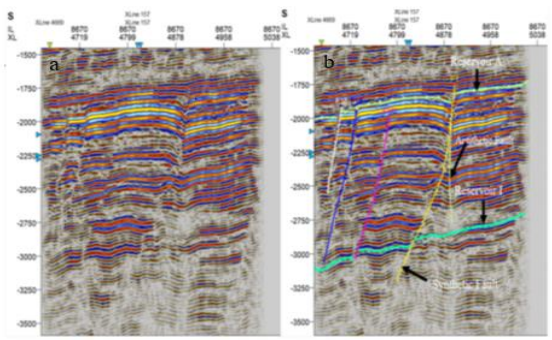

Figure 4. Faults and Horizons Interpreted Along Seismic section (a) Original Seismic, (b) Faults and Horizons Interpreted

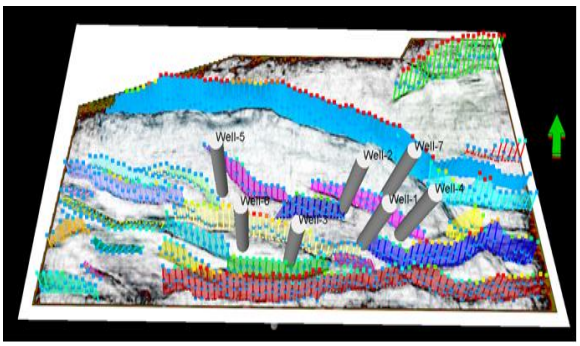

Figure 5. Interpreted Faults Displayed on the Variance Time Slice

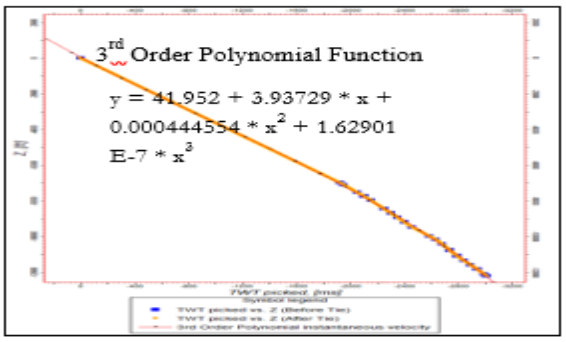

Figure 6. Third Order Polynomial Velocity model Utilized for Converting Reservoir Surfaces from Time to Depth

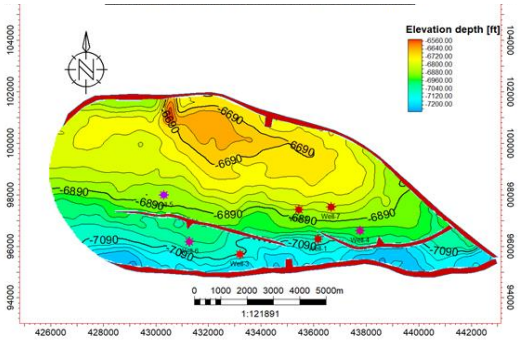

Figure 7. Reservoir Surface for Depth Surface A

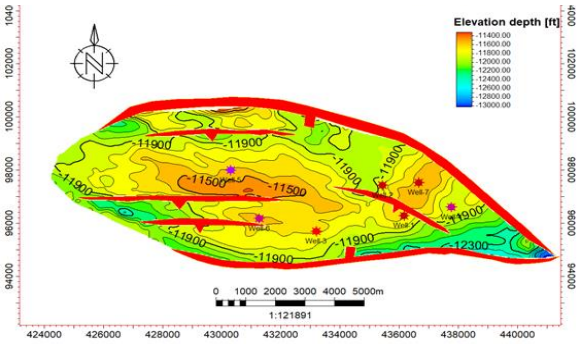

Figure 8. Reservoir Surface for Depth Surface I

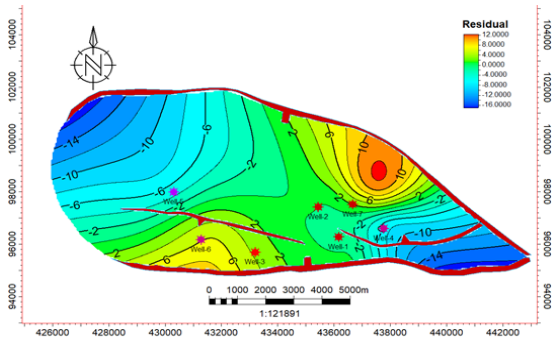

Figure 9. Depth Residual Maps Generated from Surfaces Converted Using the 3rd Order Polynomial Velocity Function for Reservoir A

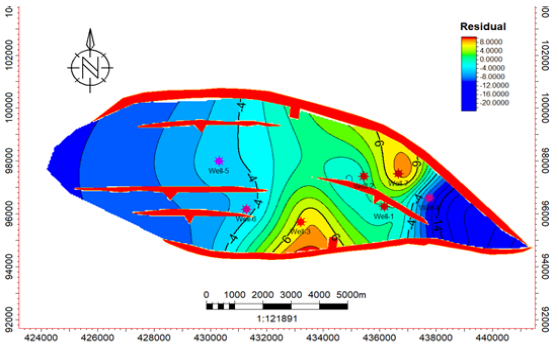

Figure 10. Depth Residual Maps Generated from Surfaces Converted Using the 3rd Order Polynomial Velocity Function for Reservoir I

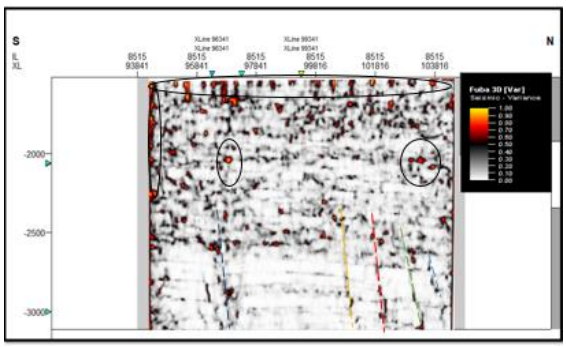

Figure 11. Variance Edge Inline 8515

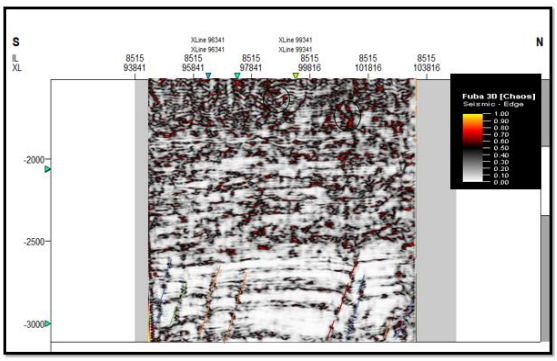

Figure 12. Chaos inline 8515

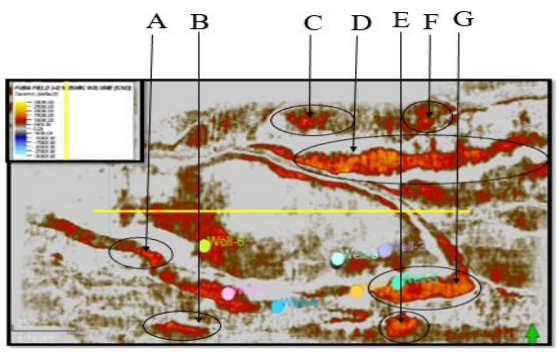

Figure 13. The General Spectral Decomposition Volume at Frequency of 12-35Hz Indicating the Prospect Zones

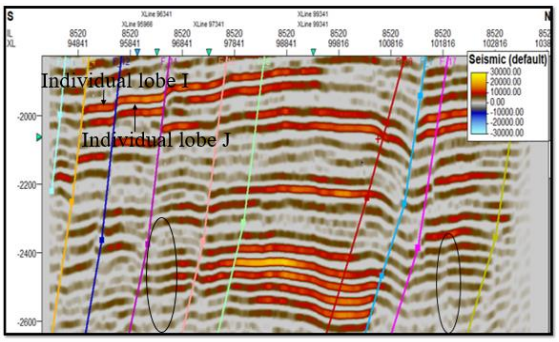

Figure 14. The General Spectral Decomposition at Frequency of 12-35Hz for Base Inline 8820

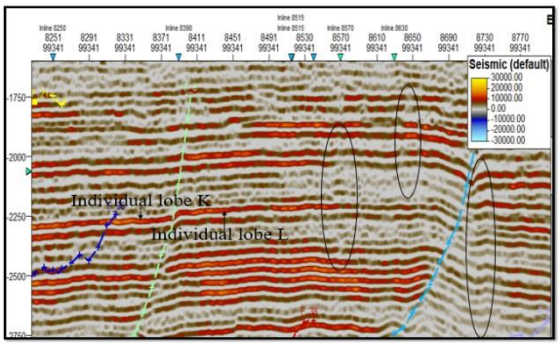

Figure 15. The General Spectral Decomposition at Frequency of 12-35Hz for Monitor Inline 8820

On Figure 2, the sands are coloured yellow while shales are grey in colour. The results for well-to-seismic tie conducted on Fuba field using density log, sonic log and checkshot of Well-1 is presented in Figure 3. A statistical wavelet (ISIS time) was used to give a near perfect match between the seismic and synthetic seismogram.

4.2. Fault and Horizon Interpretation

The results for the interpreted faults in Fuba field are presented in Figure 4 shows both synthetic and antithetic faults interpreted along seismic inlines. Faults are more visible along the inline direction because this direction reveals the true dip position of geologic structures. The variance time slice was used to validate the interpreted faults as shown in figure 5. All interpreted faults are normal synthetic and antithetic faults. A total of twenty-nine faults were interpreted across the entire seismic data. Of the interpreted faults, only F1 (synthetic fault) and F16 (antithetic fault) faults are regional, running from the top to bottom across the field. Hence, these faults play significant roles in trap formation at the upper, middle and lower sections of the field. The results for the interpreted seismic horizons (Horizons A and I) are also presented in Figure 4. On these horizons, the fault polygons were generated and eliminated. The horizons were used as inputs for the generation of reservoir time surfaces.

4.3. Depth Surfaces

The result of depth conversion residual analysis is presented in Table 1. The depth residual is the difference between the depth values of the well top from each well and the depth value from the depth converted reservoir surfaces. The depth residual analysis revealed that surfaces converted using the linear velocity function had the largest residuals ranging from -31.60 to +61.67 and from -50.58 to +40.84ft in reservoir A and reservoir I respectively. This is closely followed by the residual values obtained with the 2nd order polynomial function. The third order polynomial function shows the least residuals, ranging from -6.69 to +6.61 ft in reservoir A, and -9.48 to +8.42ft respectively. The negative depth residual indicates that the depth conversion process displaces the reservoir to a greater depth than where it occurs in the subsurface, while a positive depth residual signifies that the depth converted result has placed the reservoir at a shallower depth (Ogbamikhumi and Aderibigbe, 2019). The resultant depth residual values generated using the various velocity models (linear, 2nd and 3rd order polynomials) were compared in order to select the most suitable velocity model for depth conversion of the reservoir surfaces. Figure 6 shows the 3rd order polynomial velocity model which was selected and used as most suitable velocity model for converting A and I reservoirs from time to depth because it has the least residuals. The depth converted reservoir A

and I surfaces are presented in Figures 7 and 8 for the third order polynomial velocity function. The depth structure maps reveal that the reservoirs are anticlinal and fault supported. Reservoir A is found at a shallower depth from 6500 to 7500 ft while reservoir I is found at a deeper depth ranging from 11500 to 13000ft respectively. The depth residuals recorded from the various well locations were used to generate depth residual maps which are presented in Figures 9 and 10 respectively. The depth residual maps revealed that higher residuals on reservoir A and I surfaces are associated with the eastern and western regions which are areas not penetrated by any well.

4.4. Variance (Edge Detection) Method and Chaos

Figure 11 shows the computed variance attributes of the seismic section while Figure 12 shows the computed chaos attributes. The variance and the chaos values range from 0.0 to 1.0. Values of variance equal to 1 represent discontinuities while a continuous seismic event is represented by the value of 0. The high values are denoted with red to yellow colorations.

On the variance map and the chaos map, the areas dotted with blue, green, orange and pink colored lines signify values that correspond to the location of the discontinuity. The discontinuities may be interpreted as faults and boundaries as shown by the lines drawn on both attribute maps (Law and Chung, 2006). Both the variance edge and the chaos enhanced the faults or sedimentological bodies within the seismic data volume but the chaos enhanced the faults more. Furthermore, several bright spots are also delineated (in black circles and black ovals) which indicate high reflectivity sediments compared to their surroundings. These bright spots are an indication that a potential hydrocarbon trap might exist in the area. The darkest regions in the seismic section, which make vertical strips, may be interpreted as faults or fractures. The zones with low variance and chaos values are due to similar seismic traces. Areas with red patches represent lineaments/discontinuities while grey areas represent the structural framework of the field.

4.5. Spectral Decomposition

The general spectral decomposition was done at frequencies between 12Hz and 35Hz for the seismic. Figure 13 is the seismic volume obtained for the general spectral decomposition. Figure 13 illustrates Red-Green-Blue blend of the higher resolution of the frequency between 12Hz and 35Hz. The RGB colour blend effect gives a better understanding of the reservoirs geology. The colour blend is spectral balancing which recompense for wavelet and energy loss. The figure showed a complex meandering system and other less winding channels which are discontinuous and difficult to resolve on the seismic. The RGB colour blending slices revealed more hidden structures compared with what is observed in the time structural map. In this figure, the areas in red color indicate areas of low frequency and high amplitude associated with known hydrocarbon zones and when one colour is dominating, it showed that the frequency is dominating at that point. It revealed the geometry of the channels and other fewer sinusoidal channels. The channels are displayed with bright colouration which contains multiple frequencies as observed within the low frequency and high amplitude (indicated in black circles in Figure 13). At the north-eastern to the south-eastern part and south- western directions, there is high amplitude, an indication of hydrocarbon/gas effect. The acoustic impedance within the gas-bearing sand is lower compared to the surrounding shale (Naseer, and Asim, 2017). These are likely traps for hydrocarbon accumulation which are probable locations

for drilling new wells of economic quantity; the portions of the field are where the thin beds are. This is very important in hydrocarbon exploration wells. The amplitude response which is dominated by blue colour is high frequency. At parts where there's a change in colour to brownish, it showed thickening up of the reflectors and greater contribution from the lower frequencies. There are colour changes in the channel system which could be indicative of changes in lithology.

4.6. Stratigraphic Contact

A major geologic feature was observed on the time-slice from the divergent pattern on the seismic section as we penetrate deeper, which is an unconformity (Figures 14 and 15). This represents a significant break in vertical velocity or breaks in deposition time or record on horizon (Neuendorf, et al, 2005). This type of unconformity is called angular unconformity. Angular unconformity is an unconformity between two groups of rocks whose bedding planes are not parallel or in which the older underlying rock dips at a different angle (usually steeper) than the younger, overlying strata. Its interpretation depends on the recognition of characteristic reflection geometries rather than on amplitude information. It shows that deposition of the sediments took place at different times. Some of the lobes are indicated in Figures 14 and 15 (individual lobes I, J, K and L).

As can be seen in the areas in black ovals in Figures 14 and 15, the results of spectral decomposition at frequencies between 12Hz and 35Hz indicate the following: (a) There is more continuity of faults than previously interpreted; (b) The presence of small scale faults in the field.

Table 1. Depth Residual between Well Tops and Resultant Depth Surfaces

Reservoir/ Well	**Well Top (ft)**	**Depth Surface (ft)**	**Difference (ft)**	**Depth Surface (ft)**	**Difference (ft)**	**Depth Surface (ft)**	**Difference (ft)**
		Linear Velocity Function		***2nd Order Polynomial***		***3rd Order Polynomial***	
Reservoir A Well-1	-7054.07	-7079.08	25.01	-7032.58	-21.49	-7053.13	-0.95
Well-2	Missing	Missing	Missing	Missing	Missing	Missing	Missing
Well-3	-6877.06	-6849.08	-27.98	-6886.40	9.34	-6880.86	3.80
Well-4	-6977.93	-7039.60	61.67	-7004.73	26.80	-6971.24	-6.69
Well-5	-6905.39	-6873.79	-31.60	-6859.58	-45.81	-6900.65	-4.74
Well-6	-7065.18	-7105.10	39.92	-7028.91	-36.27	-7070.87	5.69
Well-7	-6846.24	-6877.44	31.20	-6854.65	8.41	-6852.85	6.61
Reservoir I Well-1	-11690.91	-11720.12	29.21	-11674.22	-16.69	-11690.91	0.00

Well-2	-11823.41	-11780.54	-42.87	-11807.54	-15.87	-11823.41	0.00
Well-3	-11650.06	-11684.44	34.38	-11666.36	16.30	-11656.67	6.61
Well-4	-11887.08	-11845.26	-41.82	-11912.42	25.34	-11877.60	-9.48
Well-5	-11599.86	-11549.01	-50.85	-11581.29	-18.57	-11595.11	-4.75
Well-6	-11569.00	-11534.94	-34.06	-11586.60	17.60	-11564.27	-4.73
Well-7	-11551.91	-11592.75	40.84	-11534.64	-17.27	-11560.33	8.42

5.0. Conclusion

A total of nine sand bodies (A, B, C, D, E, F, G, H and I) were identified and correlated across all seven wells in the field. Two horizons (A and I) were selected for the study. Structural interpretation of seismic data revealed that the field is highly faulted with synthetic and antithetic faults which are in line with faults trends identified in the Niger Delta. Fault and horizon interpretation revealed that closures found are collapsed crestal structures bounded by two major faults. The depth structure maps reveal anticlinal faults. Reservoirs are found at a shallower depth from 6500 to 7500 ft and at a deeper depth ranging from 11500 to 13000ft. The synthetic and antithetic faults act as good traps for the hydrocarbon accumulation in the study area. The variance and chaos values range from 0.0 to 1 .0 The Variance edge analysis and chaos were used to delineate the prominent and subtle faults in the area. The results of spectral decomposition at frequencies between 12Hz and 35Hz indicate the following: (a) some thin pay sand zones reservoirs which were characterized by of low frequency and high amplitude associated with known hydrocarbon zones, six new probable zones (Prospects A, B, C, D, E and F) of hydrocarbon accumulation were identified. (b) The presence of meandering channels, lobes and small scale faults in the field. The result showed the validity of the technique and can also be used to propose a new drilling site. Modern exploration technology with enhanced oil recovery techniques can be successfully adopted to harness the hydrocarbon in these by-passed zones where drilling was once uneconomic. This will further lead to an increase in the productivity within the field. Finally, it is recommended that further studies should be done on comparison of spectral decomposition methods in the study area.

Declarations

Source of Funding

This research did not receive any grant from funding agencies in the public, commercial, or not-for-profit sectors.

Competing Interests Statement

The author declares no competing financial, professional, or personal interests.

Consent for publication

The author declares that she consented to the publication of this research work.

Acknowledgements

The author is grateful to Shell Petroleum Development Company of Nigeria (SPDC), Port Harcourt Nigeria for the release of the academic data for the purpose of this study.

References

[1] Sheriff, R.E. (2002). Encyclopedic Dictionary of Applied Geophysics, Fourth Edition, Society of Exploration Geophysicists.

[2] Bayowa, G.O., Adagunodo A.T., Oshonaiye O.A. & Boluwade, S.B. (2021). Mapping of Thin Sandstone Reservoirs in Bisol Field, Niger Delta, Nigeria Using Spectral Decomposition Technique. Geodesy and Geodynamics, 12: 54–64.

[3] Helal, A., Farag, K.S.I., & Shihataa, M.I. (2015). Unconventional Seismic Interpretation Workflow to Enhance Seismic Attributes Results and Extract Geobodies at Gulf of Mexico Case Study. Egyptian Journal of Geology, 59: 1–14.

[4] Rotimi, O.J., Ameloko, A.A. & Adeoye O.T. (2010). Application of 3-D Structural Interpretation and Seismic Attributes Analysis to Hydrocarbon Prospecting over X-field, Niger Delta. International Journal of Basic and Applied Science, 10(4): 28–40.

[5] Doust, H. & Omatsola, E. (1990). Niger Delta, in: Edwards, J.D. & Santogrossi P.A. (Eds.), Divergent/Passive Margin Basins. AAPG Memoir, Tulsa, American Association of Petroleum Geologists, 48: 239–248.

[6] Oluwadare O.A., Olowokere M.T., Taoili F., Enikanselu P.A. & Abraham-Adejumo R.M. (2020). Application of Time-Frequency Decomposition and Seismic Attributes for Stratigraphic Interpretation of Thin Reservoirs in "Jude Field", Offshore Niger Delta. AIMS Geosciences, 6(3): 378–396.

[7] Naseer, M.T. & Asim S. (2018). Characterization of Shallow –marine Reservoirs of Lower Eocene Carbonates, Pakistan: Continuous Wavelet Transforms-based Spectral Decomposition. Journal of Natural Gas, Science and Engineering, 56: 629–649.

[8] Tayyab M.N., Asim, S. Siddiqui M.M., Naeem, M., Solange, S.H. & Babar F.K. (2017). Seismic Attributes Application to Evaluate the Goru Clastics of Indus Basin, Pakistan. Arab Journal of Geoscience, 10(7): 158.

[9] Castagna, J.P. & Sun, S. (2006). Comparison of Spectral Decomposition Methods. First Break, 24: 3–24.

[10] Taner, M.T., Koehler, F. & Sheriff, R.E. (1979). Complex Seismic Trace Analysis. Geophysics, 44: 1041–1063.

[11] Marfurt, K.J. & Kirlin R.L. (2001). Narrow-band Spectral Analysis and Thin-Bed Tuning. Geophysics, 66: 1274–1283.

[12] Sinha, S., Routh, P.S. & Anno, P.D. (2005). Spectral Decomposition of Seismic Data with Continuous Wavelet Transform. Geophysics, 70: 19–25.

[13] Tomasso, M., Bouroullec, R. & Pyles D.R. (2010). The Use of Spectral Recomposition in Tailored Forward Seismic Modelling of Outcrop Analogs. AAPG Bulletin, 94: 457–474.

[14] Whiteman, A. (1982). Nigeria: Its Petroleum Ecology Resources and Potential. London, Graham and Trotman.

[15] Adegoke, O.S., Oyebamiji, A.S., Edet, J.J, Osterloff, P.L. & Ulu, O.K (2017). Cenozoic Foraminifera and Calcareous Nannofossil Biostratigraphy of the Niger Delta. Elsevier, Cathleen Sether, United States.

[16] Short, K.C. & Stable A.J. (1967). Outline of Geology of Niger Delta. Bulletin of America Association of Petroleum Geologists, 51(5): 761–779.

[17] Horsfall, O.I., Uko, E.D., Tamunoberetonari I. & Omubo-Pepple, V.B. (2017). Rock-Physics and Seismic-Inversion Based Reservoir Characterization of AKOS FIELD, Coastal Swamp Depobelt, Niger Delta, Nigeria. IOSR Journal of Applied Geology and Geophysics, 5(4): 59–67.

[18] Ochoma, U., Uko E.D. & Horsfall, O.I. (2020). Deterministic Hydrocarbon Volume Estimation of the Onshore Fuba Field, Niger Delta, Nigeria. IOSR Journal of Applied Geology and Geophysics, 8(1): 34–40.

[19] Pigott. J.D., Kang, M.I.H. & Han, H.C. (2013). First Order Seismic Attributes for Clastic Seismic Facies Interpretation: Examples from the East China Sea. Journal of Asian Earth Science, 66: 34–54.

[20] Cohen L. (1989). Time-frequency Distributions-a Review. Proc. IEEE., Pages 941-981.

[21] Ogbamikhumi, A., & Aderibigbe, T.O. (2019). Velocity Modelling and Depth Conversion Uncertainty Analysis of Onshore Reservoirs in the Niger Delta Basin. Journal of the Cameroon Academy of Sciences, 14(3): 239–247.

[22] Naseer, M.T., Asim, S. (2017). Detection of Cretaceous Incised Valley Shale for Resource play, Miano gas field, SW Pakistan: Spectral Decomposition Using Continuous Wavelet Transform. Journal of Asian Earth Science, 147: 358–377.

[23] Neuendorf, K.K.E., Mehl, J.P. & Jackson, J.A. (2005). Glossary of Geology, Fifth Edition. American Geological Institute, Alexandria, Virginia, Page 779.